IL NUOVO CIMENTO Vol. 36 C, N. 2 Marzo-Aprile 2013
DOI 10.1393/ncc/i2013-11506-6

Colloquia: Nanoforum 2012

Selective infrared emitters based on randomly oriented silver nanowires

M. C. Larciprete([1])(*), R. Li Voti([1]), G. L. Leahu([1]), A. Belardini([1]), F. Mura([1]), C. Sibilia([1]) and A. Albertoni([2])

([1]) *Dipartimento di Scienze di Base ed Applicate per l'Ingegneria, Sapienza Università di Roma Via A. Scarpa 16, 00161 Roma, Italy*
([2]) *IR Detection Division, BFi OPTiLAS Italy - Via E. De Marchi 27, 00144 Roma, Italy*

ricevuto il 7 Marzo 2013

Summary. — We investigated randomly oriented silver nanowires films deposited onto different substrates for infrared emission reduction in the long-wavelength range, *i.e.* 8–12 μm. For this aim we prepared a set of films differing in both metallic nanowires' dimensions, length and diameter, as well as metal content. Several films were prepared by drop-casting from density-controlled solutions and then characterized by scanning electron micrography. Following this preliminary characterization, the metal filling factor for each film was retrieved using a software based on visual method. All samples were then placed onto a heating holder and their temperature evolution was monitored with a focal plane array (FPA) infrared camera, in order to characterize their infrared emission in the long infrared range. Experimental results show that the combination of wire diameter and metal filling factor may affect the infrared emission of the resulting mesh, making these coatings suitable for infrared signature reduction applications.

PACS 78.67.Uh – Nanowires.
PACS 78.66.Bz – Metals and metallic alloys.
PACS 61.46.Km – Structure of nanowires and nanorods.
PACS 78.20.Ci – Optical constants.

1. – Introduction

Absorbance and emittance in the infrared (IR) range is meeting increasing interest since its tailoring and managing [1-4] is a critical task for sensing, thermophotovoltaics as well as for security applications. Metallic nanowires have already found several applications ranging from plasmonics [5] to nonlinear optics [6-8] and the manipulation of

(*) E-mail: mariacristina.larciprete@uniroma1.it

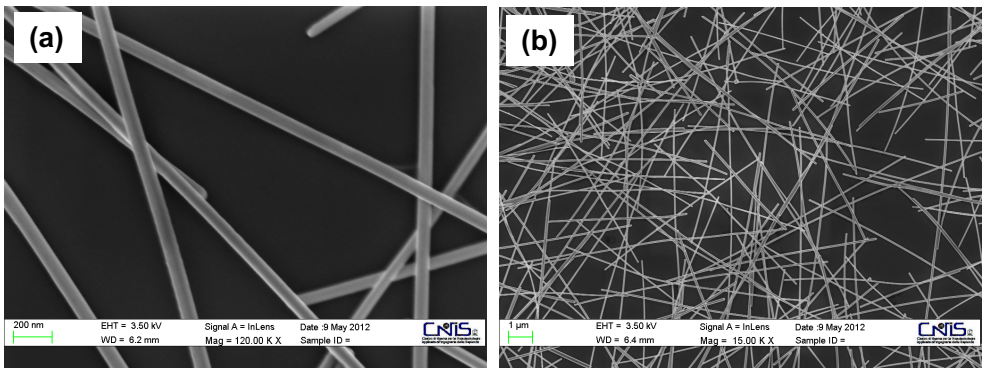

Fig. 1. – Scanning electron micrographs of long-type silver nanowires (film NW3, see table I) deposited onto silicon substrate: the wire diameter (a) and length (b) can be retrieved using suitable magnitude, respectively.

IR radiation [9], to name some. By definition, metallic nanowires have cross-sectional diameters included between few to hundreds nanometers, while their lengths span from hundreds of nanometres to some hundreds μm. Films composed by metallic nanowires may pertain high optical transmittance in the visible range, connected to the extremely reduced dimension of wires diameter, while still allowing for good electrical conduction [10], thus being suitable for all those applications where transparent electrodes are required [11].

Metallic nanowires meshes display optical properties depending on both metal filling factor and wires orientation, thus they can be employed to tune the effective optical constants and get peculiar absorbance spectra. We are specifically interested in the reduction of thermal emission in the long wavelength infrared range, 8–12 μm.

We prepared different films composed by silver nanowires, randomly oriented in the horizontal plane, deposited onto different substrates. The composed structures were characterized through scanning electron micrography (SEM) and their infrared emission was measured using a focal plane array (FPA) infrared camera operating in the long wavelength infrared range, showing the tuning of infrared emission with different filling factor.

2. – Sample preparation and characterization

Films were drop-casted starting from different suspensions of Ag-nanowires in isopropanol (IPA) (25 mg/ml), purchased from Seashell Technology, having different nanowires' length and diameter. A small amount of the starting IPA dispersion, corresponding to approximately 0.1 ml, was added to either 50 or 100 ml of deionized water. Afterwards, the Ag-nanowires suspensions were ultrasonicated for few minutes, and then filtrated and transferred onto a glass substrate by drop casting, with a procedure similar to that described in [12, 13].

Nanowires geometrical parameters, as length and diameter, were retrieved from both productor's certificate of analysis and from high resolution SEM images of the obtained films. As an example, we show in fig. 1 two SEM images obtained from sample NW3, where wires diameter (fig. 1a) and length (fig. 1b) can be determined. Following this morphological characterization, we obtained samples parameters that are thus summarized in table I, while we evaluated an averagely distributed error bar of about $\pm 10\%$.

TABLE I. – *Geometrical parameters and filling factor of the Ag nanowires films deposited onto glass substrate.*

Sample	Diameter (nm)	Length (μm)	Filling factor
NW1	60	14	≈ 0.50
NW2	55	12	≈ 0.30
NW3	100	10	≈ 0.20

The sketch of the obtained films, with the wires randomly oriented in the horizontal plane, is schematically illustrated in fig. 2.

All films were then investigated by scanning electron micrography (SEM), thus quantitative characterization of the resulting metal content film was performed with a matlab software based on visual method: the software acquires SEM images, whereas each pixel corresponds to an intensity value. Very different intensity values hold for either nanowire or substrate background, respectively, thus the silver to background fraction can be retrieved by setting an opportune intensity threshold. In fig. 3 we show two different scanning electron micrograph images obtained from a film deposited onto glass (fig. 3a) and silicon (fig. 3b) substrate, respectively. It is worth noting that changing the substrate does not affect nanowires morphology, although wires appear quite different using either a conducting (silicon) or insulating (glass) substrate. Specifically, differences in image contrast result from electrostatic charge accumulation onto insulating substrate.

3. – IR characterization

The amount of infrared radiation emitted by the metallic meshes under heating conditions was measured using a calibrated IR-camera (*i.e.* radiometric camera) and compared to the infrared emission of the bare heat source.

Samples were placed onto a hotplate holder, acting as the heat source, allowing maximum heating temperature +200 °C with fast heating-up by powerful integrated electrical heater, homogenous temperature distribution and over-temperature protection inside the plate. Setting the temperature of the integrated heater was allowed through a clear analog display, with a resolution of ≈ 10 °C. Once the hotplate temperature is fixed with

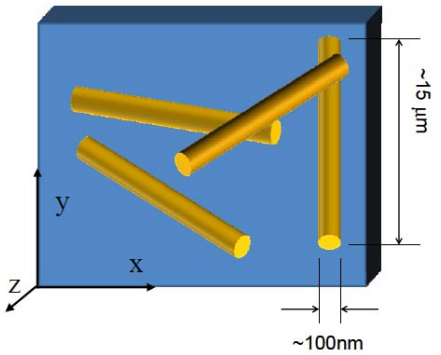

Fig. 2. – Schematic representation of the proposed nanowires based infrared absorber.

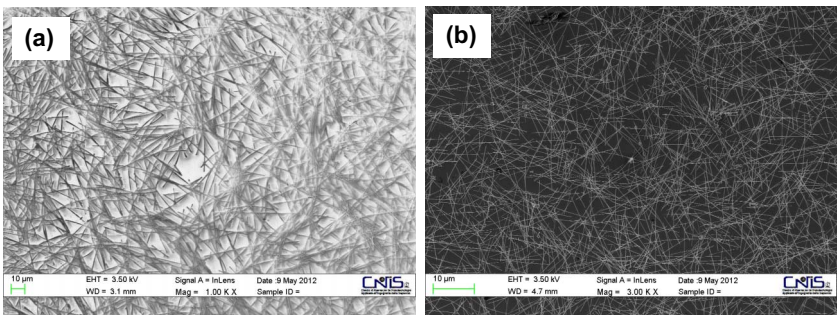

Fig. 3. – Scanning electron micrographs of long-type silver nanowires films (NW3, see table I) deposited onto different substrates: (a) glass and (b) silicon substrate, respectively.

this resolution, its actual temperature was accurately read by the IR camera, which is described in the following, as well as with a thermocouple.

A radiometric forward-looking infrared camera (FLIR) operating in the long-wavelength infrared range was used to measure the amount of infrared radiation emitted by the nanowires samples, providing detailed images of their apparent temperature. The FPA sensor of this radiometric imaging system consists in a grid of 320×256 vanadium oxide (VO_x) uncooled microbolometer, with a characteristic pixel size of $25\,\mu$m (pitch) and a noise equivalent temperature difference (NETD) of 80 mK. In order to prevent detector saturation, the temperature of sample holder was never exceeding 70 °C. The temporal evolution of both heating and cooling processes was systematically monitored by recording a set of consecutive infrared images, with a time step of 10 seconds. Samples were placed in direct contact with the heating holder, with wires' coatings facing the infrared camera, in order to avoid film deterioration.

Spurious signals arising from thermal reflection generated on the sample surface by external environmental sources was avoided by using black opaque shields to protect the camera/sample setup and to confine the complete camera field of view (FOV).

An example of a typical radiometric image, where the three Ag-nanowires samples are observed in the meantime, is shown in fig. 4. This image was recorded at the fixed

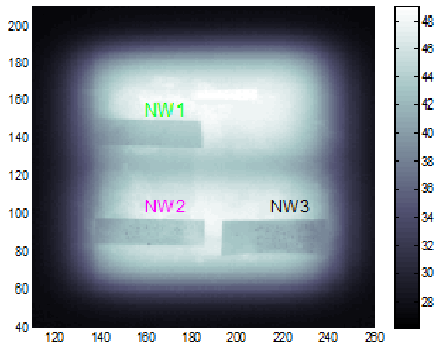

Fig. 4. – Example of an infrared image recorded with a long-wavelength IR camera at heating temperature of about 50 °C. The three different samples are evidenced with corresponding labels.

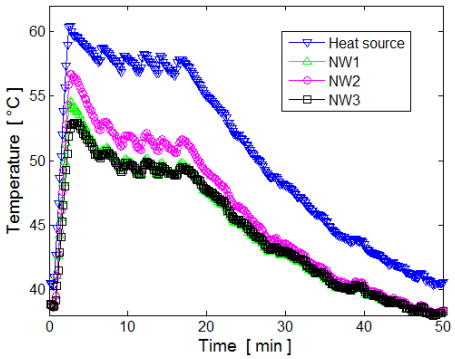

Fig. 5. – Experimental plot of temperature evolution as a function of time, measured in the LWIR range, *i.e.* 8–12 μm, for the three different silver nanowires samples (see table I), during heating and cooling process.

temperature of $\approx 50\,^{\circ}$C. The different samples are evidenced with capital letters. The colorbar at the right side quantifies the amount of IR radiation reaching the camera's microbolometers, in other words the infrared signal integrated between 8 and 12 μm. It can be easily recognized that the intensity level corresponding to the nanowires samples, namely NW1, NW2 and NW3, appear to be darker, with respect to the intensity level arising from the heating substrate, *i.e.* despite the temperature rise, the infrared images of Ag nanowires films only display a weak bleaching, with respect to the underlying hotplate.

The set of consecutive radiometric images was then examined by means of a MatLab software, thus the IR signal values were retrieved from the images data. For each sample an uniform area was selected over the radiometric images and those data arising from the corresponding pixels were numerically integrated so to obtain the mean value of the resulting IR intensity level, which also corresponds to the resulting apparent temperature. The obtained data are reported in fig. 5, where the resulting apparent temperature is given as a function of time. According to the temperature values reported for the heating holder, samples were heated during the first five minutes, then the temperature was kept constant for about fifteen minutes, and afterwards the current was switched off to observe the cooling phase.

The experimental curves show that under heating conditions of about 60 °C, the apparent temperature of all the nanowires films show a trend similar to the corresponding heating holder temperature, having all curves the same shape. On the other hand, considering their absolute values, the apparent temperature of the three samples always keeps below that of the heat source, although with some differences among them, NW2 reaching the highest temperature, and NW1 and NW3 being somewhat lower.

4. – Results and discussions

The different values of the experimental curves can be interpreted by retrieving the permittivity corresponding to each nanowires film. In principle the permittivity values of such a composite are strongly affected by the morphology (nanowires) and surface effects. Although it is hard to retrieve its accurate spectral values, an effective medium model can be employed for a comparison of the absorbance between the nanowires film and silver ($f = 1$).

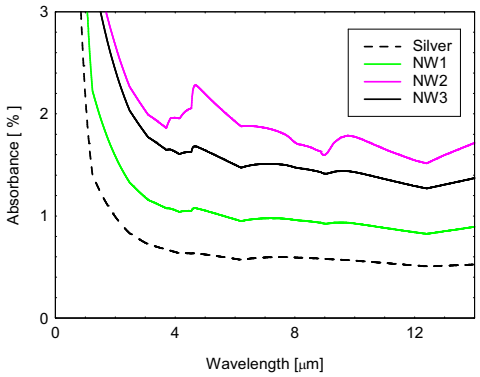

Fig. 6. – Plot of the calculated absorbance spectra using refractive index and extinction coefficient, for the three nanowires' samples, whose data are reported in table I. For all calculated curves, the substrate is glass.

Considering an effective medium with silver nanowires randomly aligned in the xy-plane (see fig. 2), its permittivity presents a dyadic form, where $\varepsilon_{xx} = \varepsilon_{yy}$ lay in the plane of the wires and ε_{zz} is in the direction perpendicular to film surface. Briefly, the relative permittivity of such an effective medium can be calculated by using the mixing formulas for randomly oriented ellipsoidal inclusions reported in [14], as a function of the metal filling factor, f. The following expressions are obtained for the transverse $\varepsilon_{xx} = \varepsilon_{yy}$, and for the perpendicular dyadic components, ε_{zz}:

$$\varepsilon_{xx} = \varepsilon_{yy} = \varepsilon_e + \frac{f}{2}\varepsilon_e\left(\varepsilon_i - \varepsilon_e\right)\frac{\dfrac{1}{\varepsilon_e} + \dfrac{1}{\varepsilon_e + \left(\varepsilon_i - \varepsilon_e\right)/2}}{1 - \dfrac{f}{4}\dfrac{\left(\varepsilon_i - \varepsilon_e\right)}{\varepsilon_e + \left(\varepsilon_i - \varepsilon_e\right)/2}}, \tag{1}$$

$$\varepsilon_{zz} = \varepsilon_e + f\left(\varepsilon_i - \varepsilon_e\right), \tag{2}$$

where ε_e and ε_i are the relative permittivities of the host matrix and the wires, respectively. We considered a medium composed of air-surrounded nanowires, thus $\varepsilon_e = 1$, while the optical constants of silver were taken from [15].

The metal filling factor is evaluated from SEM top-view images by means of the colour contrast between the area of silver (area_{Ag}) or air (area_{air}). These values are then employed to calculate $f = \text{area}_{\text{Ag}}/\text{area}_{\text{air}}$, with an estimated uncertainty of about $\pm 5\%$.

Since the radiometric emission was detected at normal incidence, *i.e.* perpendicularly to films' surface, we assume that the radiation polarization is equally distributed along the xy-plane. Following these considerations, the real and imaginary part of the permittivity components, $\varepsilon_{xx} = \varepsilon_{yy}$, were calculated for the three different silver nanowires meshes in the whole IR investigated range. Next, the refractive index and extinction coefficients were retrieved for the silver nanowires systems, being $\text{Re}(\varepsilon) = n^2 - k^2$ and $\text{Im}(\varepsilon) = 2nk$, and used to recover the spectral absorbance A from Kirchhoff's law $A = 1 - |T|^2 - |R|^2$, where T is the transmission coefficient and R is the reflection coefficient, obtained by applying the transfer matrix method.

In fig. 6 these results are summarized for the three different films, whose thickness is assumed to be proportional to wires' diameter. It is notable that the combination of

different thickness and filling factor may produce different absorbance dispersion, which in turns result in a different trend of the experimental curves. In particular, we note that sample NW1, having the highest metal content ($f \approx 0.5$), presents the lower absorbance values within the whole investigated wavelength range. On the other hand, the sample NW2, due to the lower filling factor combined with its thickness value, show the highest absorbance values, in agreement with experimental data. Finally, for sample NW3 absorbance value, the low metal filling factor ($f \approx 0.2$) is compensated by the highest thickness (100 nm). Similar measurements were performed also on the silver nanowires films deposited onto silicon substrate, and concordant experimental results are reported elsewhere. As a reference, we also show the absorbance spectra calculated for a silver film, 60 nm thick.

Both experimental results and theoretical studies reflect the fact that metals in general pertain very high reflectance values in the IR range. As a consequence, for a metal-based film, the higher the metal content, in terms of either thickness or filling factor, the lower the absorbance in the IR range. In other words, as the film metal content increases, its dielectric constant value becomes closer to that of pure silver, which behaves-in the IR-as a mirror.

5. – Conclusions

In conclusions, we investigated randomly oriented silver nanowires films deposited onto different substrates in order to characterize their IR emission under heating conditions in the wavelength range 8–12 μm. In particular, we reported experimental results obtained from a set of films deposited onto glass, differing in both metallic nanowires' dimensions, length and diameter, as well as metal content. Samples' temperature evolution was observed using a focal plane array (FPA) infrared camera, evidencing that silver nanowires films keep an apparent temperature which is always below that of the driving heat source. The different experimental curves were interpreted usign effective permittivity calculations, as a function of metal filling factor in the corresponding film. The obtained results indicate that randomly oriented silver nanowires meshes allow the thermal camouflage of the underlying heat source. As a further development, the apparent temperature read by the IR camera can also be intentionally heterogeneous, *i.e.* by preparing films with variable wires concentration.

REFERENCES

[1] Mattiucci N., D'Aguanno G., Alu A., Agryropoulos C., Foreman J. V. and J. B. M., *Appl. Phys. Lett.*, **100** (2012) 201109.
[2] Li Voti R., Larciprete M. C., Leahu G., Sibilia C. and Bertolotti M., *J. Appl. Phys.*, **112** (2012) 034305.
[3] Li Voti R., Larciprete M. C., Leahu G., Sibilia C. and Bertolotti M., *J. Nanophoton.*, **6** (2012) 061601.
[4] D'Aguanno G., Larciprete M. C., Mattiucci N., Belardini A., Bloemer M. J., Fazio E., Buganov O., Centini M. and Sibilia C., *Phys. Rev. A*, **81** (2010) 013834.
[5] Sun Y., *Nanoscale*, **2** (2010) 1626.
[6] Belardini A., Larciprete M. C., Centini M., Fazio E., Sibilia C., Chiappe D., Martella C., Toma, A. and G. M. and Buatier De Mongeot F., *Phys. Rev. Lett.*, **107** (2011) 257401.
[7] Belardini A., Larciprete M. C., Centini M., Fazio E., Sibilia C., Toma A., Chiappe D. and Buatier De Mongeot F., *Optics Express*, **17** (2009) 3603.

[8] Belardini A., Pannone F., Leahu G., Larciprete M. C., Centini M., Sibilia C., Martella C., Giordano M., Chiappe D. and Buatier De Mongeot F., *Appl. Phys. Lett.*, **100** (2012) 251109.
[9] Larciprete M. C., Albertoni A., Belardini A., Leahu G., Li Voti R., Mura F., Sibilia C., Nefedov I., Anoshkin I. V., Kauppinen E. I. and Nasibulin A. G., *J. Appl. Phys.*, **1112** (2012) 083503.
[10] Madaria A., Kumar A., Ishikawa F. N. and Zhou C., *Nano Research*, **3** (2010) 564.
[11] Michelotti F., Belardini A., Larciprete M. C., Bertolotti M., Rousseau A., Ratsimihety A., Schoer A. and Mueller J., *Appl. Phys. Lett.*, **83** (2003) 4477.
[12] Toschi F., Orlanducci S., Guglielmotti V., Cianchetta I., Magni C., Terranova M. L., Pasquali M., Tamburri E., Matassa R. and Rossi M., *Chem. Phys. Lett.*, **539** (2012) .
[13] Terranova M. L., Manno D., Rossi M., Serra A., Filippo E., Orlanducci S. and Tamburri E., *Crystal Growth Design*, **9** (2009) 1245.
[14] Sihvola A. H., *Electromagnetic Mixing Formulas and Applications. IEEE Electromagnetic Wave Series*, **47** (IEEE Publishing, London) 1999.
[15] Palik E. D., *Handbook of optical constants of solids* (Academic Press, Inc. New York) 1985.